Decline of the Critical Period of Visual Plasticity Is Concurrent with the Reduction of NR2B Subunit of the Synaptic NMDA Receptor in Layer 4

Alev Erisir and Janna L. Harris
Department of Psychology, University of Virginia, Charlottesville, Virginia 22904-4400

The specific composition of NMDA receptor subunits is thought to underlie the developmental plasticity of the cortex revealed by unbalanced binocular stimulation. However, evidence that NR2 subunits change in correlation with the critical period at locations that are relevant to visual plasticity has been missing. Using preembedding and postembedding immunostaining, as well as electron microscopy, we quantified the volumetric densities of NR1-, NR2A-, and NR2B-containing synapses in layers 4 and 2/3 of the ferret visual cortex at different postnatal ages. Before eye opening, NR2A is encountered infrequently at postsynaptic sites in layer 4, but it increases sharply by postnatal day 34. In the subsequent weeks, postsynaptic NR2A labeling increases gradually in both layers 4 and 2/3 to become the most prevalent subunit in the adult animal. The NR2B subunit is the more prevalent subunit at the onset of the critical period of cortical plasticity. However, it displays different developmental patterns in layers 4 and 2/3. Although no change occurs in synaptic NR2B density in layer 2/3, in layer 4, NR2B maintains its high levels through the peak of the critical period and then becomes significantly reduced by the end of the peak of the critical period. This low level is maintained throughout adulthood. Our results demonstrate a correlation between the loss of NR2B subunits from layer 4 synaptic sites and the decline of the critical period, suggesting that the presence of NR2B subunits at synaptic sites could be a permissive factor regulating the ocular dominance plasticity of the developing cortex.

Key words: **NR2A; NR2B; NMDA receptor; synaptic density; developmental plasticity; quantification; ultrastructure; electron microscopy; ocular dominance; ferret**

Introduction

During an activity-dependent critical period, external manipulations impair the formation of ocular dominance columns and the refinement of thalamocortical connections in the visual cortex (Hubel et al., 1977; LeVay et al., 1980). Blockade of the NMDA-type glutamate receptor (NMDAR) reduces the effects of monocular deprivation (Kleinschmidt et al., 1987; Gu et al., 1989; Bear et al., 1990; Rauschecker, 1991; Roberts et al., 1998), suggesting that NMDAR function maintains plasticity.

However, a demonstration that NMDARs are present in the visual cortex in a manner that allows plasticity during the critical period, but not after its end, has been required. Although obligatory subunit NR1 expression is fairly stable over development, NR2 subunits draw particular attention; long-duration, NR2B-mediated currents characterize early development, whereas NR2A-mediated short-duration currents and NR2A protein expression become more prevalent as the animal ages (Williams et al., 1993; Monyer et al., 1994; Sheng et al., 1994; Portera-Cailliau et al., 1996). However, reports on the time frame of these changes have been conflicting: NR2A increases drastically (Roberts and Ramoa, 1999; Chen et al., 2000) or moderately (Cao et al., 2000a) at the onset of the critical period or gradually increases from birth to juvenile ages (Quinlan et al., 1999). Meanwhile, NR2B maintains the high levels found at birth throughout and beyond the critical period (Roberts and Ramoa, 1999), increases gradually (Quinlan et al., 1999), or transiently declines at the end of the critical period (Cao et al., 2000a). It has also been argued that the critical factor may be an increase in the NR2A/NR2B ratio, rather than the amounts of the subunits, because this can reduce the plasticity by decreasing the open time of the channel and thus Ca^{2+}-activated processes (Carmignoto and Vicini, 1992; Flint et al., 1997, Roberts and Ramoa, 1999). However, whereas the increase of the NR2A/NR2B ratio is closely correlated with the shortening of cortical NMDA currents, the increase in the ratio of NR2 subunits occurs at the onset, or throughout the critical period at best, without a significant change during the time that plasticity diminishes (Quinlan et al., 1999; Roberts and Ramoa, 1999). Because no sustained correlation between loss of plasticity and the amounts of the receptors or ratios of the subunits is detected, evidence implying a reduced function of NMDARs in ending the critical period has remained elusive. Nevertheless, because the NMDAR continues to be the most plausible constituent of plasticity throughout the brain, a more detailed examination of NR2 subunit distribution is warranted.

The aforementioned anatomical studies examining the temporal expression pattern of NR2 subunits have at least one of two shortcomings: (1) an inclusion of nonsynaptic receptor proteins in the quantification and (2) analysis of all of the cortical layers together. The receptor proteins at nonsynaptic sites, such as somatic or dendritic cytoplasm, may constitute a large portion of the total protein synthesized. Therefore, quantifications that do

Received Oct. 9, 2002; revised March 17, 2003; accepted March 26, 2003.

This work was supported by National Eye Institute Grant R01-EY12138 to A.E. We thank Lucien Alexandre and Jacqueline Tweedy for excellent technical support and Dr. Chiye Aoki for her input at the beginning of this project.

Correspondence should be addressed to Dr. Alev Erisir, University of Virginia, 102 Gilmer Hall, P.O. Box 400400, Charlottesville, VA 22904-4400. E-mail: erisir@virginia.edu.

 0270-6474/03/235208-11$15.00/0

not differentiate between synaptic and cytoplasmic proteins (Roberts and Ramoa, 1999; Cao et al., 2000a) potentially overlook the changes that may be occurring at postsynaptic sites. It is possible that only the synaptic proteins can truly reflect the functional changes. Similarly, the preparation of all of the cortical layers combined (Quinlan et al., 1999; Chen et al., 2000) may have the inherent drawback of generalizing the changes occurring in the entire cortex to those relevant to ocular dominance plasticity. NMDARs are used by glutamatergic circuitry throughout the cortex; however, ocular dominance plasticity most probably concerns a specific circuit and not the entire cortex. A laminar analysis of synaptic NR2 subunits has not been presented in the literature.

To fill this gap, we examined layer 4 (thalamocortical input layer) and layer 2/3 of the ferret visual cortex for patterns of synaptic NMDAR subunit localization. The use of electron microscopy (EM) allowed us to concentrate on particular layers and to control for changes in synaptic density and brain volume that occur as the animals mature. Our results provide evidence that synaptic localization of one subunit, NR2B, displays a dramatic reduction at the end of the critical period in layer 4 but not in the supragranular layers.

Materials and Methods

We examined brain tissue from 10 ferrets at the ages of postnatal day 27 (P27), P34, P43, P46, P56, P60 (two ferrets), postnatal month 3 (two ferrets), and adulthood. All of the procedures were approved by institutional animal welfare committees and were in accordance with the guidelines of the National Institutes of Health. The ages of the ferrets were chosen to represent periods before the onset of the critical period, the onset of the critical period, the peak of the critical period, the end of the critical period, and the adult ages. The choice of ages was based on the critical period of the ferret visual cortex, as defined by Issa et al. (1999). These investigators have shown the effect of monocular deprivation on the monocularity of cells recorded in layers 2/3, 4, 5, and 6 of the ferret visual cortex. They have shown that monocular deprivation initiated by P42 produced the largest effects (peak of the critical period), whereas those initiated between P50 and P65 were approximately one-half as effective (end of the critical period), and concluded that the critical period of ocular dominance lasts between P35 and P60 (see Fig. 7) (Issa et al., 1999). They also reported that the critical period ends somewhat (~1 week) earlier in layer 4 than in the other layers (see Fig. 2*D*) (Issa et al., 1999). Therefore, we considered the data collected from P55–P60 brains representing the end of the critical period in layer 4 of the visual cortex of ferrets.

Preparation of visual cortex tissue. All of the ferrets were given an overdose of Nembutal and perfused transcardially with heparinized saline for 2 min, followed by a mixture of 4% paraformaldehyde and 1% glutaraldehyde for 30 min. Fixatives were dissolved in 0.1 M phosphate buffer (PB) at pH 7.4. After perfusions, the brains were extracted, and the blocks containing visual cortices were dissected and immersed in the same fixative overnight. A vibratome was used to cut sections (60–100 μm thick) coronally through the visual cortex. Every 13th section was mounted on a gelatin-coated slide for Nissl staining. The remaining sections were treated with 1% $NaBH_4$ to terminate the cross-linking actions of the fixatives and stored free-floating in 0.01 M PBS containing 0.05% sodium azide at 4°C.

Preembedding immunocytochemistry. The sections were rinsed and treated in 1% bovine serum albumin (BSA) in PBS for 30 min. They were then incubated in a 10 μg/ml dilution of polyclonal rabbit anti-NR2A or -NR2B (Upstate Biotechnology, Lake Placid, NY) or a 1:500 dilution of monoclonal anti-NR1 (PharMingen, San Diego, CA) in PBS with 1% BSA, for 3 d at room temperature. A 0.05% dilution of sodium azide was added to the incubation medium to prevent bacterial growth. After incubation in the primary antibody, the sections were rinsed and incubated in a biotinylated goat anti-rabbit or goat anti-mouse secondary antibody (Vector Laboratories, Burlingame, CA) for 2 hr, followed by a 2 hr incubation in HRP-conjugated avidin–biotin complex (ABC; Vector Laboratories). Immunoreactivity was visualized using diaminobenzidine (DAB) (0.05%) and H_2O_2 (0.001%). For all of the antibodies, deletion of the primary antibody eliminated all of the specific staining discernible at the EM level.

Embedding. Preembedding immunostained sections were fixed with 2% glutaraldehyde in PB for 10 min and with 1% osmium tetroxide for 1 hr. Then the sections were dehydrated in a series of alcohols and embedded in resin (Embed 812; Electron Microscopy Sciences, Fort Washington, PA) using procedures described previously (Chan et al., 1990; Locke, 1994). The sections to be immunostained with the postembedding technique were treated using an osmium-free method described by Phend et al. (1995). Briefly, the sections were rinsed in 0.1 M maleate buffer and treated in 1% tannic acid for 40 min, followed by incubations in 1% uranyl acetate for 40 min and 0.5% iridium tetrabromide for 20 min, with maleate buffer rinses between the incubations. Then the sections were dehydrated in a series of alcohols, in which three 70% alcohol rinses were interlaced with 1% *para*-phenylenediamine for 15 min and 1% uranyl acetate for 30 min. Finally, the sections were rinsed in acetone and infiltrated with Epon–Spurr by incubating them in increasing concentrations of acetone–resin mixture.

All of the sections that went through the steps of fixation and resin infiltration were flat embedded between two pieces of Aclar sheet (Ted Pella, Redding, CA), and the resin was allowed to polymerize either overnight (Embed 812) or for 3 d (Epon–Spurr) at 60°C. Then the sections were drawn with the aid of a camera lucida, and the areas to be analyzed by EM were chosen, cut, and placed on flat surfaces of Beem capsule caps. These capsules were then filled with resin and left in the 60°C oven until the resin in the capsule polymerized. An ultramicrotome (Leica Ultracut UC7; Leica, Nussloch, Germany) was used to cut ultrathin sections that were oriented near parallel to the surface of the sections cut by the vibratome and that contained sample from all of the cortical layers. This approach maximizes the area of tissue–Epon interface, at which most of the penetration of antibody can be expected within the initial ultrathin sections, and therefore permits the efficient detection of immunolabeled profiles. Sections were examined on Jeol (Peabody, MA) 1200XL or Jeol JEM1010 microscopes.

Postembedding gold immunocytochemistry. We used a postembedding immunogold procedure that was described previously by Erisir et al. (1997a) and modified from Phend et al. (1992) to label profiles in a given section for NR2A or NR2B. Briefly, after the sections were embedded in Epon–Spurr and cut, the grids containing ultrathin sections were rinsed for 5 min in Tris-buffered saline with 0.1% Triton X-100 (TBST) at pH 7.6 and incubated in a 100 μg/ml dilution of anti-NR2A or anti-NR2B in TBST for 2 hr. They were then rinsed and incubated for 1 hr in a 1:35 dilution of goat anti-rabbit IgG conjugated to gold particles (GAR15; Ted Pella) in TBST at pH 8.2. The sections were rinsed in TBST and in distilled water and fixed in 2% glutaraldehyde (EM grade; Electron Microscopy Sciences) for 10 min. Some sections were counterstained with 2% lead citrate to increase ultrastructural contrast.

Analysis. Light microscopy was used to determine the borders of the cortical layers on the resin-embedded sections. For this, typically, a capsule-embedded section was drawn using a camera lucida, and certain landmarks, such as labeled cells, myelinated axon bundles, and blood vessels, were marked. This drawing was first compared with near-adjacent Nissl-stained sections and then was used to determine the position of the targeted cortical layer (layer 4 or 2/3) that was to be examined by EM on ultrathin sections collected from the same capsule-embedded section.

For quantitative EM analysis, the synapse was used as the main counting unit. From each brain that was stained with the preembedding technique, at least 10 nonoverlapping photographs were taken at 10,000 or 12,000× magnification. The negatives were digitized and examined at 35,000× final magnification using Image-Pro Plus 4.0 software (Media Cybernetics, Silver Spring, MD). On each photograph, with systematic sweeps, each synapse was located, and its length was measured. Then, the experimenter judged whether the presynaptic or postsynaptic elements of the synapse contained any label and evaluated the type of synaptic

contact (symmetric or asymmetric) and the type of postsynaptic element (dendrite shaft, spine, or soma).

The identification of synapses and postsynaptic profiles was performed with the following considerations. The criteria to identify a synapse were the presence of at least one synaptic vesicle in contact with a plasma membrane, at least three more vesicles within the same profile (this criterion allowed identification of the profile as a presynaptic terminal), and the parallel alignment of the postsynaptic plasma membrane with that of the terminal. Neither clear visualization of a synaptic cleft nor the presence of presynaptic or postsynaptic densities was considered a necessary criterion; both type 1 and type 2 synapses were included in the counting. The length of the synapse was measured along the parallel-aligned plasma membranes. If the synapse was perforated, synaptic length included the length of the perforation; the incidence of a terminal bouton contacting two different postsynaptic profiles was treated as two different synapses. The postsynaptic profile was classified as a spine, a dendritic shaft, or a cell body. A dendritic shaft was identified by the presence of microtubules organized in parallel or by the presence of mitochondria, and the cell bodies were identified by the presence of an endoplasmic reticulum, subsynaptic cisterna, the Golgi apparatus, or a nucleus. Profiles that did not fit in either the dendrite or cell category were identified as spines.

The area represented in each photograph was measured, excluding the blood vessels, myelinated axons, and cell bodies. The areal density of synapses (N_A indicates number of synapses per area) was calculated and used to find the volumetric density of synapses ($N_V = N_A$/average synaptic length) (Colonnier and Beaulieu, 1985; DeFelipe et al., 1999). This calculation is based on the assumption that the average synapse is spherical in shape. The average length of all of the synaptic profiles in a photograph therefore represents the average diameter of the synapses and the average depth, perpendicular to the plane of the section, of the volume effectively represented by the two-dimensional image. The volumetric density of the labeled profiles was also calculated using a similar formula that took into account only the labeled synapses. To calculate the prevalence of labeled profiles over the total area examined, the average volumetric density of labeled synaptic profiles was divided by the average volumetric density of all of the synaptic profiles (labeled and unlabeled), and the fraction was expressed as a percentage.

For the analysis of sections stained with the postembedding gold technique, we examined the ultrathin sections from each age group on the electron microscope, counting the number of labeled and unlabeled synapses in each section. For each asymmetric synapse encountered, the lack or the presence of one, two, or three or more gold particles directly on the postsynaptic membrane and the synaptic cleft was noted. The ratio of labeled synapses (either those containing one or more gold particle on the synapse or those containing more than one particle, depending on the cutoff criteria) to all of the synapses was calculated and expressed as a percentage.

Preparation of photographic plates. To prepare illustrations containing photomicrographs, EM negatives (3 × 4 inches) were scanned at 5800 dots per inch (dpi) to yield photographs of desired dimensions at 1200 dpi. Using Adobe Photoshop 5.5 (Adobe Systems, San Jose, CA), the brightness of the photographs was adjusted to obtain a uniform white level in all of the photographs in a plate; no contrast adjustments were performed. Light microscope images were captured using a digital camera (DC200; Leica, Nussloch, Germany) at 1272×10^{17} resolution and grayscale settings, using 20 or 60× objectives. Images were then reduced to the desired size without digital resampling, to yield photographs at 600 dpi. Adobe Photoshop was also used to place labels on the photographs.

Results

Immunostaining for NR1, NR2A, and NR2B antibodies: qualitative analysis

Light microscopy

We examined coronally cut sections of visual cortex from ferrets at the postnatal ages of P34 to adult. Antibodies for NR1, NR2A, and NR2B stained all of the layers of cortex. The light-microscopic staining patterns with the three antibodies did not

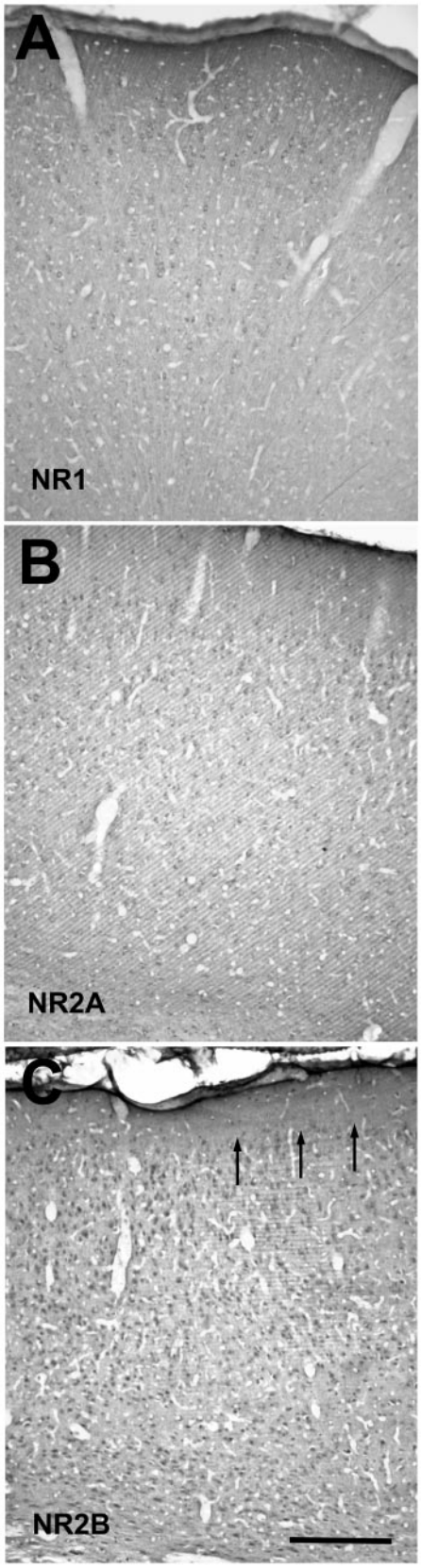

Figure 1. Light-microscopic view of coronal sections through the visual cortex of a P43 ferret, stained with NR1 (*A*), NR2A (*B*), or NR2B (*C*) antibodies. Staining is representative of that seen in all of the ages examined and does not reveal any laminar differences. Arrows in *C* mark the border between layers 1 and 2. Scale bar, 500 μm.

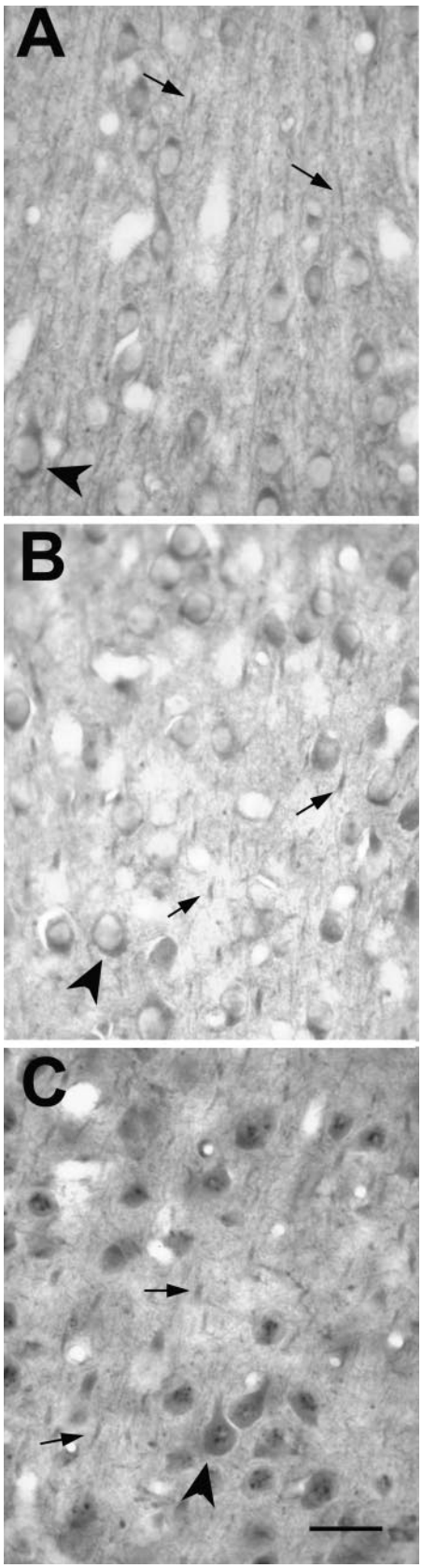

Figure 2. Light-microscopic view of staining patterns around layers 4 and 2/3 of the visual cortex, stained with NR1 (*A*), NR2A (*B*), or NR2B (*C*) antibodies. These samples are from a P43 animal and are representative of all of the ages examined. Arrowheads in all of the panels point to examples of somata staining, and arrows mark neuropil staining resolvable at light-microscopic resolution. Scale bar, 50 μm.

reveal gross differences in the localization of these receptors (Fig. 1). Light perikaryal staining was present in the cells (Fig. 2); nuclei were devoid of staining, except for aggregate deposits of chromagen in the nuclei of NR2B-stained sections (Fig. 2*C*). Extrasomatic regions showed diffuse labeling with all three antibodies. More discrete, punctate labeling was observed in longitudinally cut dendritic segments, which at times emerge from lightly labeled cells. The label was also observed as small puncta in extrasomatic regions; it can be speculated that, at light-microscopic resolutions, this kind of labeling is discrete receptor labeling or the presence of label in orthogonally cut dendrites or spines. This pattern of staining with all three antibodies was observed in all of the layers at all of the ages. No cortical layer stained differentially, except for layer 1, in which a scarcity of cell bodies naturally delineates the border.

Electron microscopy

We used two different approaches to visualize NR1, NR2A, or NR2B at the electron-microscopic level: a postembedding immunogold method and a preembedding DAB method. The general patterns of labeling using these two approaches were similar. Using the immunogold approach, NR2A or NR2B labeling was found primarily at the postsynaptic density of spines or small-caliber dendrites, contacted by terminals forming asymmetric contacts (Fig. 3). Scattered gold particles were also detected throughout the section (Fig. 3*B*). However, in contrast to synaptic gold labeling, in which the presence of a gold particle on the highly specific synapse structure can be considered a positive label, a qualitative analysis of nonsynaptic gold labeling using these receptor antibodies was not feasible because of the low cluster rate at nonsynaptic sites. However, because the ABC–DAB method is more sensitive for amplifying a weak signal, a preembedding DAB labeling method was well suited for detecting nonsynaptic sites in which NR2A and NR2B were present. On such sections, the ultrastructural sites that displayed staining were similar using all three antibodies. Label was present at postsynaptic sites in dendritic spines and small-caliber dendrites (Fig. 4), as well as in presynaptic terminals (Fig. 5*A*), cytoplasm of dendritic shafts, somatic cytosol (Fig. 5*B*), and glial processes. This qualitative localization pattern is similar to that observed by Aoki (1997) in the cat visual cortex, using NR1 immunocytochemistry for EM.

Quantitative EM analysis

Our primary aim was to quantify the amounts of NMDAR proteins at different developmental ages in layers 4 and 2/3 of the ferret visual cortex. However, we first needed to address some methodological concerns. The quantification approach we used (see Materials and Methods) yields a reliable measure of profile density in single sections (DeFelipe et al., 1999). For this calculation of volumetric density, the information on tissue thickness was derived from the average length of the synapses. This was particularly important in our developmental study because, as in any quantitative analysis performed on single sections, the sampling probability of any profile is proportional to the size of its counting unit (Erisir et al., 1997b; Van Horn et al., 2000). If the average synaptic length changes as the brain matures, this could introduce a sampling bias to a quantitative study involving animals at different ages. Therefore, we first analyzed the pattern of developmental changes in synapse morphology.

Size of synapses in layer 4 of the developing cortex

We examined a total of 8502.74 μm^2 of cortex and encountered a total of 1768 synapses from five animals at the ages of P34, P43,

P60, P90, and adult. Figure 6 shows the frequency distributions of synaptic length at these ages. An initial Kruskal–Wallis test revealed that the synaptic length distributions from the five different ages were not identical, and at least one of the population distributions was different from at least one of the others ($p < 0.0001$). Therefore, we compared the synaptic length distribution from each age with each of other ages, using a Mann–Whitney *U* analysis, and found that synaptic length distributions at P34 and P43 were significantly different from each of those from P90 and adult brains (for *p* values, see Fig. 6 legend). Similarly, the P60 synaptic length was different from that found in adult cortex. In contrast, no difference was found between P34 and P43, or P43 and P60, P60 and P90, and P90 and adult brains. Therefore, the general trend for the mean synaptic length was a gradual increase throughout the first 3 months of life (Fig. 6).

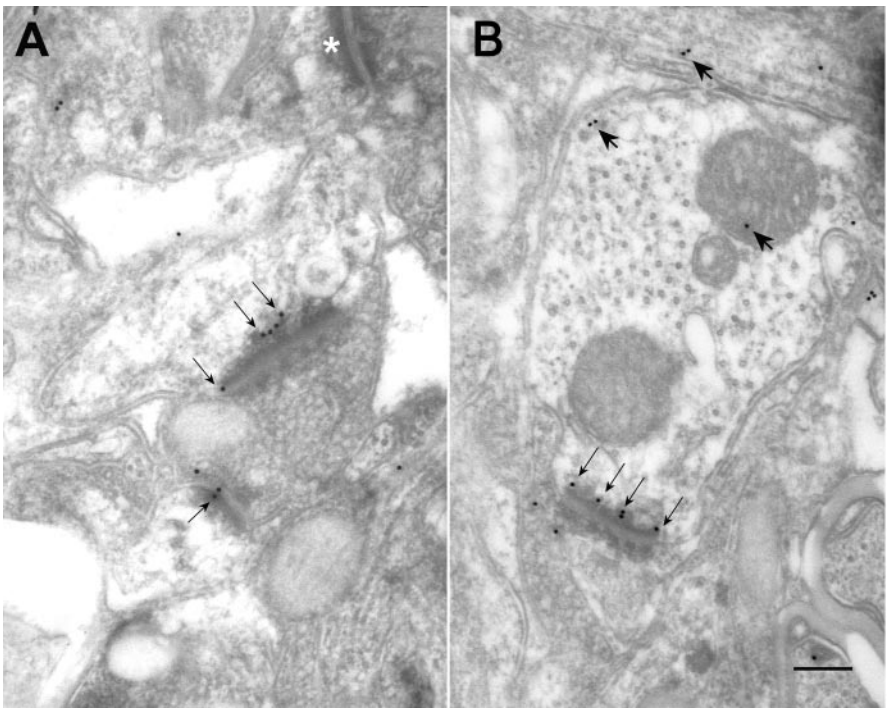

Figure 3. Electron micrographs of layer 4 of the visual cortex, stained for the presence of NR2A (*A*) or NR2B (*B*) subunits, using the postembedding immunogold procedure. Thin arrows on both panels point to gold particles on or near the postsynaptic membrane. Thick arrows in *B* indicate nonsynaptic gold labeling that can be encountered in such tissue (for details, see Results), and the white asterisk in *A* marks an unlabeled synapse. Scale bar, 500 nm.

Density of synapses in developing cortex

In ferrets, the visual cortex undergoes a drastic change in volume and structure during the first 3 months of life. Once the cortical layers are established, thalamocortical axons, as well as corticocortical glutamatergic axons, and interneuronal GABAergic axons invade the cortex to establish appropriate circuits (Katz and Callaway, 1992; Callaway and Lieber, 1996; Durack and Katz, 1996; Gao et al., 1999). Furthermore, as the postnatal brain develops, the extracellular matrix is reduced, whereas intracellular volume is increased because of the elongation of dendritic trunks, and many axons become myelinated. Because these changes could introduce a sampling bias for any quantitative study that does not find a way to account for them, we first determined the density of synapses in layers 4 and 2/3 of each brain.

This analysis showed that the synaptic density in layers 4 and 2/3 increased throughout the developmental ages. Two layers had significantly different synaptic densities at any given age, and the changes in the synaptic densities occurred at different rates. We also included measurements of synaptic density at P27 in our analysis. However, it should be noted that, at this age, the laminar borders are not yet differentiated. Therefore, our layer 4 measurements at this age are taken from the middle portion of cortical plate. P27 is characterized by a drastic scarcity of synapses, such that, by P34, synaptic density more than doubled in layer 4. After P34, synaptic densities in both layers of the visual cortex increased rapidly and reached a plateau after P60 (Fig. 7). The comparison of the pattern of synaptic density in layers 4 and 2/3 also revealed that, in P34 brain, synaptic density in layer 4 was significantly higher than that in layer 2/3 (*t* test; $p < 0.001$), and this pattern was reversed by P60, suggesting that the rate of synaptogenesis in layer 2/3 was higher than that in layer 4 during the critical period of visual plasticity (Fig. 7).

Density of labeled synapses in layer 4 of the developing cortex

We then analyzed the volumetric density of the profiles immunostained for NMDA subunits. Because the synapse density is not constant across ages, the densities of labeled synapses in each condition were normalized to the baseline synaptic density for each case. The rationale for this approach is as follows: in analysis of labeled profiles, the counting unit is the synaptic site. Thus, labeled profiles are more likely to be found in a region with plenty of synapses than in a region with fewer synapses. This fact necessitates a control for the variability of synaptic density in the regions examined. Normalizing the density of labeled profiles to the overall synaptic density for each photograph served to compensate for this sampling bias. We quantified the density of labeled synapses using the formula described in Materials and Methods. For each photograph, the number of labeled synapses per unit of area was divided by the average length of the labeled synapses, to obtain the volumetric density of labeled profiles. This measurement was in turn normalized to the total (labeled and unlabeled) synaptic density obtained for the same case. As a result, the normalized labeled synaptic densities for each antibody staining reported below are expressed as the percentage ratio of all of the synapses encountered in each case. Two hundred photographs, representing 12239.62 μm^2, were examined; the same photographs were also used in the analysis of synaptic density described above.

Calculations of the normalized density of labeled synapses showed that, at P34, shortly after eye opening and at the onset of the critical period in ferrets (Issa et al., 1999), ~47% of all of the synapses in layer 4 were immunoreactive for NR1. This measure increased over the critical period to reach ~63% at P90 (Fig. 8*A*). This temporal pattern of NR1 subunit localization is agreement with previous results.

When we examined NR2A and NR2B synaptic densities, we obtained interesting results. At P27, several days before eye opening and the onset of the critical period, NR2A-labeled profiles were a small portion of all of the synapses (~20%), whereas NR2B label was found twice as frequently (40%). By P34, NR2A

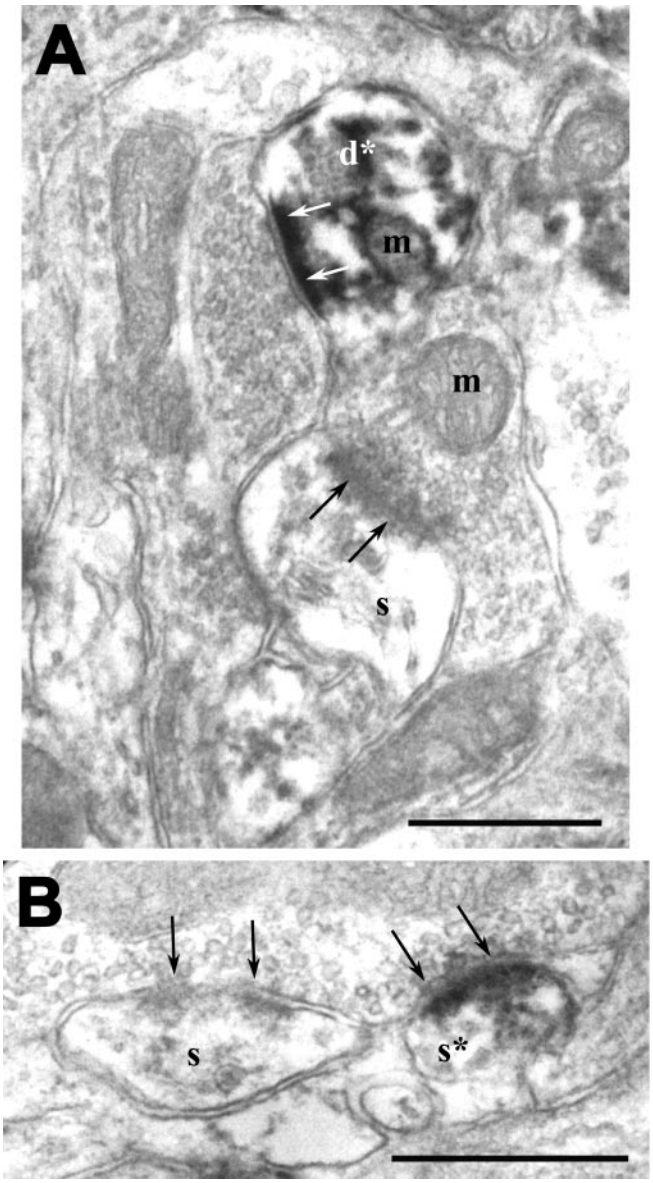

Figure 4. Postsynaptic immunolabeling in ferret visual cortex, using the preembedding DAB method. *A*, An NR2A-labeled dendrite (d*) and an unlabeled spine (s) can be seen in the same plane. Both profiles are postsynaptic to unlabeled terminals; arrows point to synapses from the postsynaptic side. The section was obtained from layer 4 of a P60 animal. m, Mitochondrion. Scale bar, 500 nm. *B*, NR2B immunostaining in a postsynaptic spine (s*) encountered in layer 2/3 of a P43 animal. This spine is postsynaptic to a terminal that forms another asymmetric synapse on an adjacent unlabeled spine (s). Arrows point to the synapse from the presynaptic side. Scale bar, 500 nm.

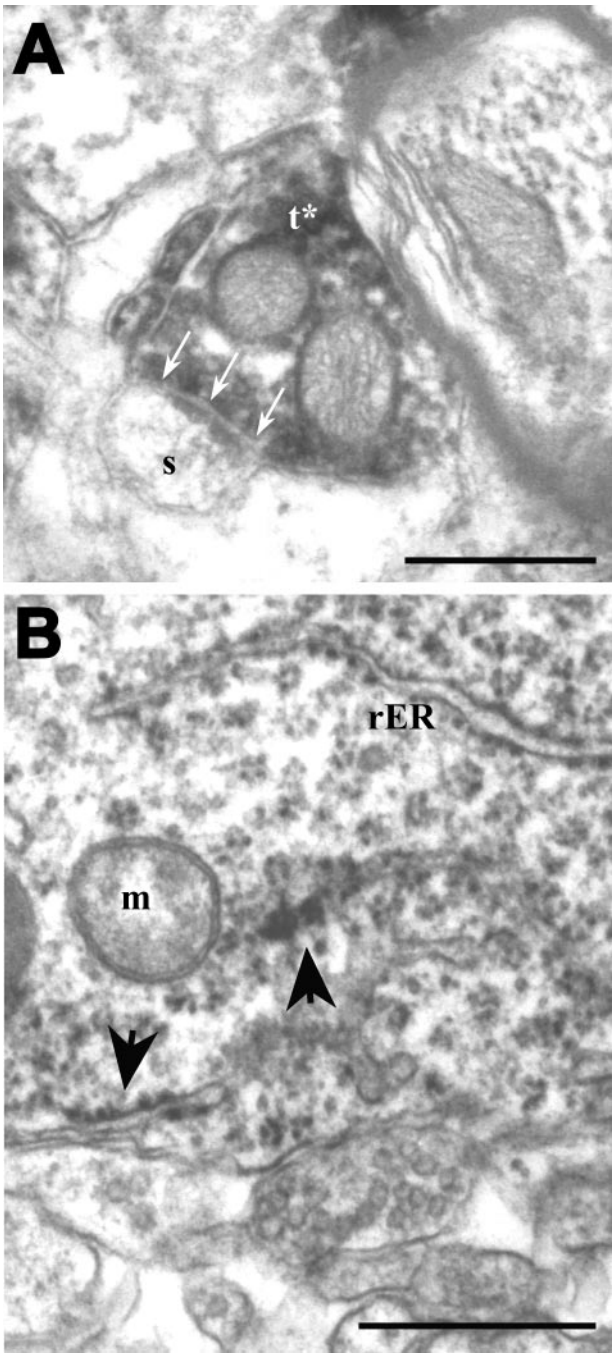

Figure 5. Receptor immunolabeling encountered in sites other than postsynaptic profiles. *A*, NR2A immunoreactivity encountered in a terminal (t*) forming an asymmetric synapse (arrows) on an unlabeled spine (s). This EM photograph was taken from layer 4 of the visual cortex of an adult ferret. Scale bar, 500 nm. *B*, EM view of layer 2/3 of the visual cortex in a P34 ferret, immunostained for NR2B. A labeled cell body occupies the field. Labeling can be seen as accumulations on rough endoplasmic reticulum (rER; arrows) and free ribosomes. m, Mitochondrion. Scale bar, 500 nm.

density was almost doubled, whereas NR2B density displayed a modest increase. Two points need to be elaborated here. The change in the NR2A density between P27 and P34 was the largest relative change that we found between any age group, and this may explain the drastic increase in NR2A-mediated currents observed in layer 4 at the onset of the critical period (Roberts and Ramoa, 1999). Second, as reported above, at the same time frame, cortical synaptic density in layer 4 also increases drastically, possibly requiring even higher rates of NR2A protein synthesis to catch up with the rate of synaptogenesis. Similarly, we do not see any reduction in NR2B-labeled synapse ratio correlated with the rate of synaptogenesis, implying that the onset of the critical period is a time when a lot of new NR2B-containing synapses are also generated.

As the animal aged, NR2A density continued to increase steadily. This increase was prominent at the height of the critical period, as well as at the end of the critical period and the adult ages (Fig. 8*B*). In contrast, as it was before the eyes opened, at the onset of the critical period, NR2B was the most prevalent subunit at synapses: 50–55% of the synapses displayed NR2B immunoreactivity. This high level was retained through the height of the critical period; however, by P56–P60, labeled synapses were re-

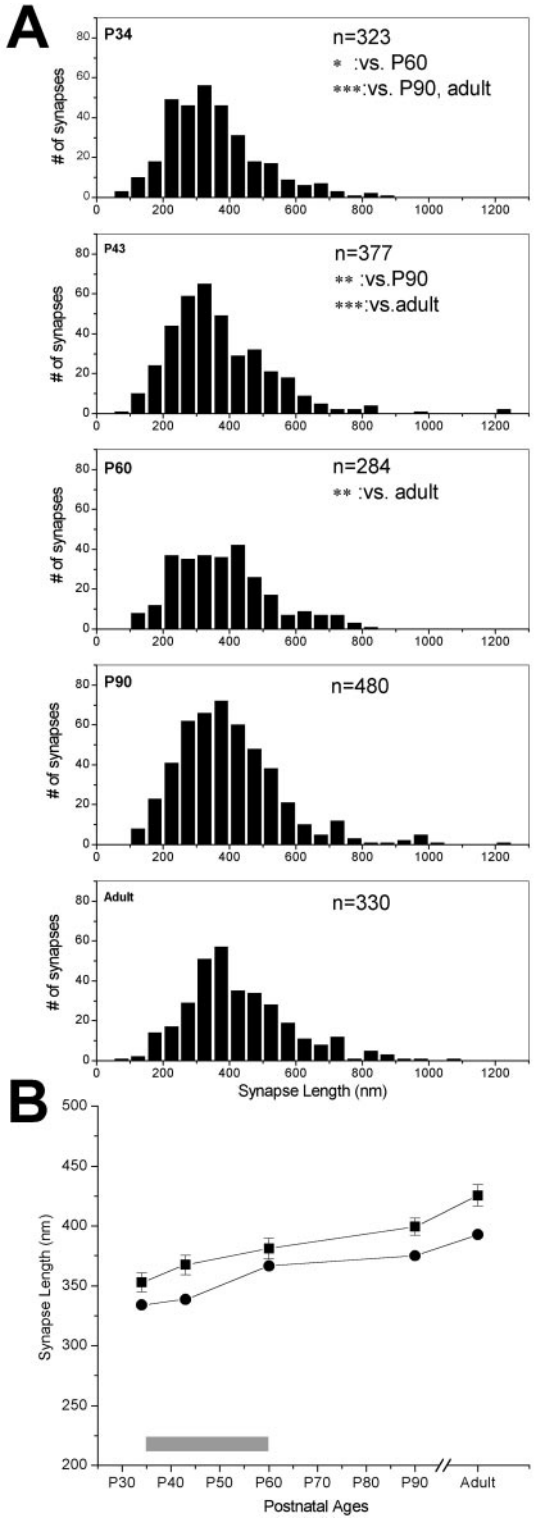

Figure 6. Changes in synaptic length over developmental ages. *A*, Frequency distribution histograms (black bars) of synaptic length measured in layer 4, at five ages. *n* values in each panel refer to the number of synapses analyzed at each age. Significance values for Mann–Whitney *U* comparisons are given in the appropriate panels: $*p < 0.01$; $**p < 0.001$; $***p < 0.0001$. *B*, Means (squares; error bars are SE of all synapses measured at each age) and medians (circles) of synaptic lengths at ages corresponding to the critical period of visual cortex plasticity (gray bar over the *x*-axis, here and in the following figures) and older ages. Note that the critical period in the ferret is determined from data from all of the ages, and the end of the peak of the critical period in layer 4 occurs ~1 week earlier than it does in all of the layers (Issa et al., 1999).

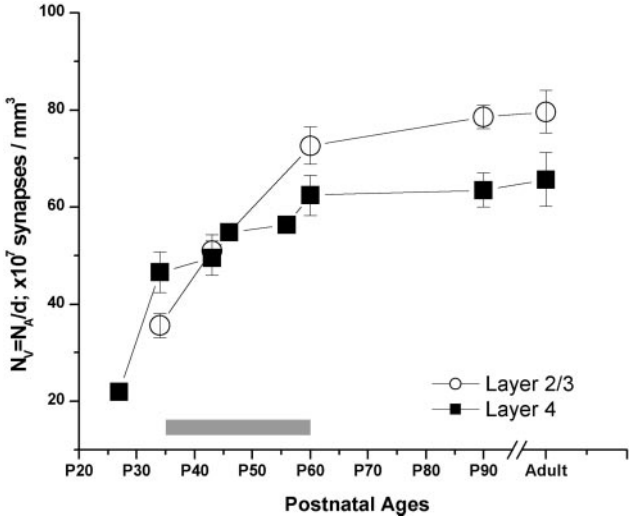

Figure 7. Average volumetric synaptic density (N_V) in layer 2/3 (open circles) and layer 4 (filled squares) of the visual cortex at five developmental ages. For this analysis, each photograph, representing 50–70 μm^2 of cortex, was used as an individual sample. Error bars represent the SE of 10–15 samples.

duced to 30%. This low ratio was maintained through P90 and adulthood (Fig. 8*C*). Although a portion of the label included in our analysis may represent polypeptides not yet inserted into the membrane, the contribution of such nonfunctional proteins to our sample is probably very small, because we were able to detect quantitative changes regardless.

Labeled synapse ratio in layer 4 using postembedding gold labeling

We also studied the prevalence of NR2A and NR2B subunits in layer 4 of the visual cortex, using sections stained with a postembedding gold procedure (Table 1). We counted a total of 939 asymmetric synapses in NR2A- and NR2B-stained ultrathin sections at P43 and P90 and computed the ratio of NR2A- or NR2B-labeled synapses to all of the synapses. The results of this analysis confirmed the findings of our volumetric density analysis: at P43, the ratio of NR2A-labeled synapses was significantly lower than that of NR2B-labeled synapses, whereas at P90, NR2A-labeled synapses became the most prominent, because the ratio of NR2B-labeled synapses was significantly reduced ($p < 0.001$; *t* test) (Fig. 9). This trend was evident both when the criterion of labeling was one or more gold particles and when it was more than one gold particle (Table 1).

Comparison of the densities of labeled synapses in layers 4 and 2/3

To address whether or not the observed decline in synaptic NR2B subunits is layer specific, we analyzed the densities of NR2A- and NR2B-labeled synapses in layer 2/3 of the developing visual cortex. We counted 1419 synapses in layer 2/3 of the visual cortex in some of the brains used in the analysis of layer 4. A total of 3902 μm^2 of brain area was analyzed, excluding somata, myelinated axons, and capillaries. The volumetric density of labeled synapses, corrected for the synaptic density in each case, showed that the NR2B subunit was more prominent than the NR2A subunit in layer 2/3 at P34. In subsequent weeks, the NR2A density increased gradually to nearly double its P34 density at P90; this pattern was similar to the changes that occurred in layer 4 (Fig. 10*A*). In contrast, the postsynaptic NR2B density remained at high levels at all of the ages; in the adult brain, the NR2A and NR2B densities were equivalent. This developmental pattern of postsynaptic NR2B labeling was significantly different from that

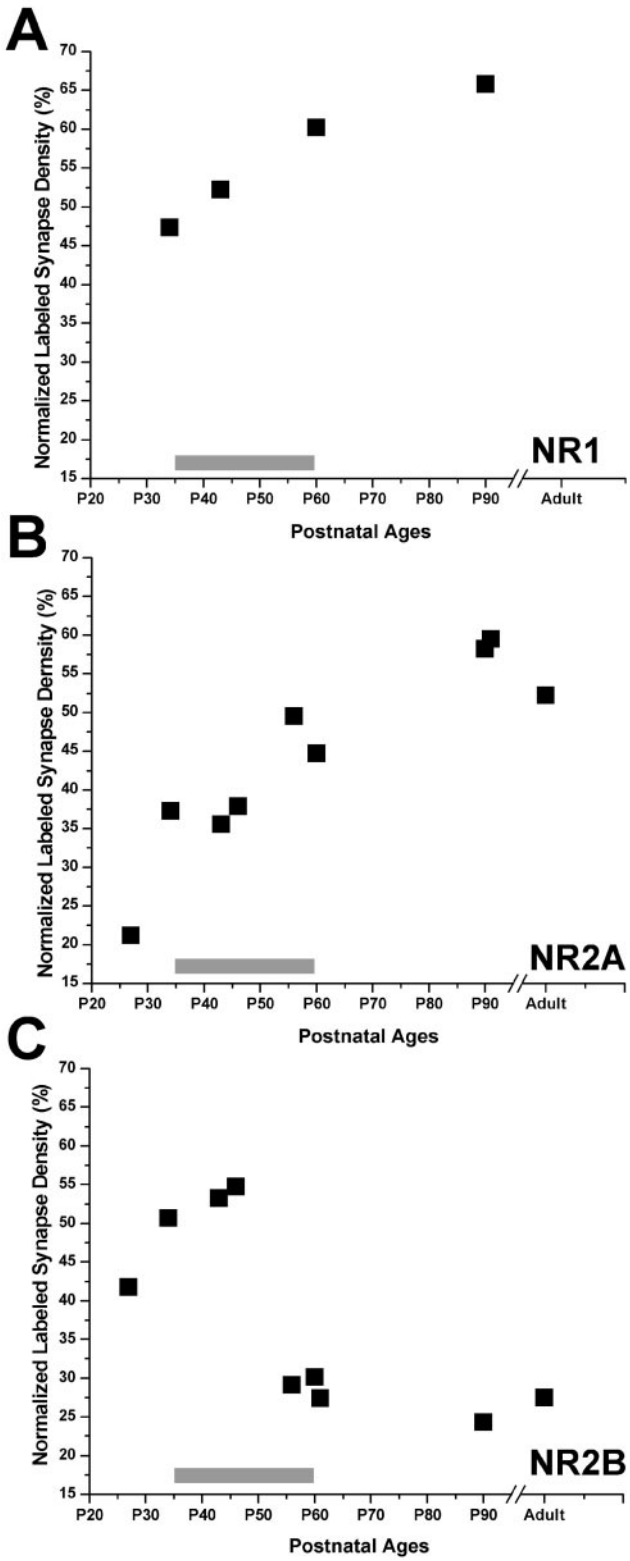

Figure 8. Normalized volumetric density (black squares) of synapses in layer 4, immunoreactive for NR1 (*A*), NR2A (*B*), or NR2B (*C*) before eye opening (P27), at the onset (P32–P38), peak (P40–P50), and end (P55–P62) of the critical period, and at adult ages.

observed in layer 4. Specifically, in layer 2/3, the end of the critical period of plasticity was not correlated with any significant change in the prevalence of the NR2B subunit (Fig. 10*B*).

To address whether the ratio of NR2A to NR2B subunit densities shows a substantial change as the plasticity declines, and if so, whether this change is sustained after the critical period, we plotted the NR2A/NR2B ratio (Fig. 10*C*). This analysis revealed that the NR2A/NR2B ratio in layer 4 indeed starts increasing as the plasticity wanes in this layer (between P45 and P55), primarily attributable to the drastic decrease in NR2B density occurring at the same time. However, this new NR2A/NR2B level is not sustained past the end of the critical period, mostly because of increasing NR2A density at later ages. In layer 2/3, the NR2A/NR2B ratio gradually increased at all of the age periods.

Table 1. Percentage of NR2A- or NR2B-labeled asymmetric synapses in layer 4 at two different ages, using two different criteria for labeling

	Percentage of asymmetric synapses having one or more gold particle	Percentage of asymmetric synapses having more than one gold particle	Number of synapses
NR2A			
P43	$22.29 \pm 0.67^{a,b}$	$8.1 \pm 0.02^{a,b}$	246
P90	56.76 ± 1.02^{b}	37.55 ± 5.07^{b}	215
NR2B			
P43	83.18 ± 4.74^{a}	68.8 ± 4.98^{a}	202
P90	23.79 ± 3.09	10.38 ± 1.64	276

$^{a}p < 0.005$, *t* test, P43 versus P90.

$^{b}p < 0.005$, *t* test, NR2A versus NR2B.

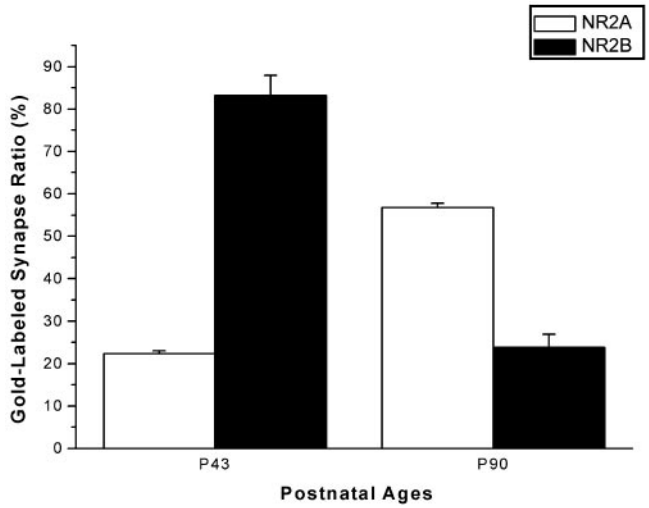

Figure 9. Prevalence of NR2 subunits in layer 4 of the visual cortex, visualized by the postembedding immunogold method. Means and the SE (averages from 3 or more sections) of the ratio of NR2A (open bars)- or NR2B (filled bars)-labeled synapses to all of the asymmetric synapses are plotted against the age.

Discussion

Our study provides evidence that the decline of developmental plasticity in the visual cortex coincides with a sharp reduction in the volumetric density of synaptic NR2B subunit of NMDARs in layer 4, suggesting that the presence of NR2B at synaptic sites could be a permissive factor for ocular dominance plasticity. This reduction is specific to layer 4; the prevalence of synaptic NR2B does not change in layer 2/3. However, the most drastic change in synaptic NR2A occurs at the onset of the critical period, after which NR2A levels gradually increase during and after the critical period in both layers studied.

Synaptic NR2A density

Our results on the density of synaptic NR2A agree with the findings that the duration of NMDA EPSCs becomes shorter at the

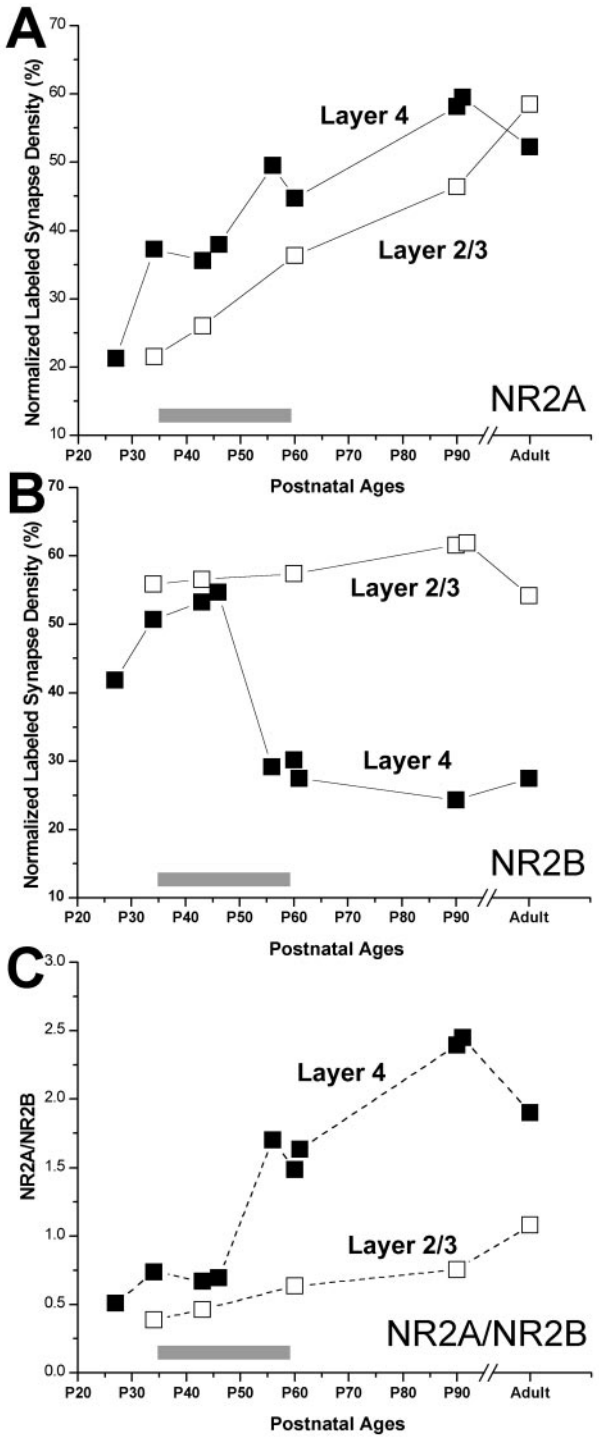

Figure 10. Comparisons of normalized volumetric density of NR2A (*A*)- and NR2B (*B*)-labeled synapses in layer 4 (filled squares; redrawn from Fig. 8) and layer 2/3 (open squares). *C*, The NR2A/NR2B ratio in layer 4 (filled squares) and in layer 2/3 (open squares). The points are connected with solid lines (in *A* and *B*) and dashed lines (in *C*) to ease viewing of individual variables.

onset of the critical period (Carmignoto and Vicini, 1992; Roberts and Ramoa, 1999) and that the shorter NMDA currents can be the outcome of the presence of NR2A subunits (Monyer et al., 1992; Flint et al., 1997). An increase in cortical NR2A protein expression during early development has been demonstrated previously (Quinlan et al., 1999; Roberts and Ramoa, 1999; Chen et al., 2000). We now demonstrate that NR2A subunits also become more prominent at layer 4 synaptic sites, providing evidence that the EPSC shortening in older animals is the result of increased incorporation of NR2A subunits into synapses.

Synaptic NR2B and plasticity

We provide the first evidence that the amount of synaptic NR2B declines concurrently with the reduction of plasticity in layer 4 of the visual cortex. The advantage of our study over previous studies in which this pattern was not evident (Quinlan et al., 1999; Roberts and Ramoa, 1999; Cao et al., 2000a,b; Chen et al., 2000) is the use of EM, which allowed us to concentrate on specific layers and to quantify only the protein located at or near the postsynaptic membrane. Layer-specific developmental patterns, such as those found in our experiments, can explain why no critical period-related change in NR2B is observed when all of the layers are combined.

Previous work in the cat visual cortex by Daw (1994) has shown that cells in layer 2/3 retain a capacity for experience-dependent ocular dominance plasticity long after cells in layer 4 have lost their plastic properties. Similarly, the critical period in the ferret visual cortex closes earlier in layer 4 than in other layers (Issa et al., 1999). Furthermore, visual and other sensory cortices display a substantial capability for activity-dependent plasticity through adulthood (Weinberger, 1995; Buonomano and Merzenich, 1998; Gilbert, 1998; Godde et al., 2002). Although the persistence of NR2B in layer 2/3 may imply that developmental plasticity requires the NR2B subunit in glutamatergic synapses, it may also be an indication of laminar differences in heteromeric NMDAR formation. Our results favor the latter possibility: as more NR2A are added into synapses, they may either form new NR1/NR2A receptors or may be inserted into preexisting NR1/NR2B receptors to form NR1/NR2B/NR2A heteromers. Both configurations would enable EPSP shortening in cortex. However, whereas the second configuration is likely to be found in layer 2/3, in which NR2B amounts are sustained despite the NR2A increase, a higher prevalence of the first configuration is expected in layer 4, in which NR2B amounts decline independent of NR2A increase. Although these predictions require confirmation using double-labeling experiments, other evidence also points to the idea that the NMDA-mediated plasticity may be regulated on a structure-specific, layer-specific, and even synapse- or input-specific manner (Philpot et al., 2001; Stern et al., 2001).

A developmental switch or specificity for individual inputs?

The decline of visual cortical plasticity has been attributed to a modification of NMDAR subunit composition. One such model proposes that the presence of more NR2A than NR2B at synapses brings the critical period for developmental plasticity to an end, possibly by reducing the Ca^{2+} entry into the postsynaptic cell. This model predicts that the number of NR1/NR2A receptors highly exceeds the number of NR1/NR2B receptors (i.e., higher NR2A/NR2B ratio) at the end of the critical period. However, there are problems in embracing this hypothesis: the largest increases in NR2A subunit amounts and in NR2A-mediated currents occur before the peak of the critical period rather than at the end (Carmignoto and Vicini, 1992; Quinlan et al., 1999; Roberts and Ramoa, 1999). Our results showing a drastic increase in layer 4 synaptic NR2A right after eye opening is in agreement with those findings. Furthermore, a recent study using knock-out mice showed that animals lacking the NR2A subunit experienced a normal critical period for barrel-cortex plasticity (Lu et al., 2001). Thus, it was suggested that regulation of NMDAR subunit

composition via NR2A synthesis was not essential for terminating cortical development.

In the present study, we tested an alternative model, proposing that the loss of NR2B-containing NMDARs from relevant and specific postsynaptic sites (possibly from the thalamocortical synapse), not the regulation of NMDAR subunit composition, is directly related to the reduction of developmental plasticity. Our results support this hypothesis: the initial increase in the NR2A/NR2B ratio at layer 4, corresponding to the period when the plasticity wanes in this layer, is primarily attributable to the reduction of NR2B and not to the addition of NR2A subunit to the synapses; the NR2A/NR2B ratio continues to increase beyond the critical period, and the only parameter that is sustained beyond the peak of the critical period is the low level of NR2B-containing NMDA receptors. The loss of the NMDAR from a particular input synapse in layer 4 would eliminate Ca^{2+} entry into the postsynaptic cell, thereby stalling the second messenger-regulated processes that may underlie the state of plasticity. Such delayed consequences of NMDAR loss may explain the residual plasticity encountered during the days after the end of the critical period peak. Furthermore, this model does not contradict physiological findings showing an increase in NR2A-mediated currents during approximately the same time as the ocular dominance plasticity is observed (Carmignoto and Vicini, 1992; Roberts and Ramoa, 1999). The increase of synaptic NR2A-containing NMDARs in general would explain the dominance of mature-type NMDA currents in the cortex, whereas the loss of NR2B-containing NMDARs from a particular input, which may constitute a considerably small fraction of all of the glutamatergic synapses, can be responsible for the loss of plasticity in ocular dominance circuits.

Site of NR2B loss

As the input primarily affected by monocular deprivation, the thalamocortical synapse is an attractive candidate for initial location of NR2B-containing NMDARs. Indeed, in layer 4, the site of thalamocortical projection, NMDA-mediated responses are the strongest in early development (Tsumoto et al., 1987; Fox et al., 1989; Lu et al., 2001), although they become more prominent in layer 2/3 in adulthood (Fox et al., 1989, 1990; Shirokawa et al., 1989; Currie et al., 1994). The presence of NR2B-containing NMDARs at thalamocortical synapses during the critical period can be the prerequisite for plastic changes that occur when visual stimuli become unbalanced, as during monocular deprivation. Our experiments show ~50% reduction in synaptic NR2B, suggesting that the loss of NR2B occurs in at least one, but not all, of the synaptic populations. In adult cats, thalamocortical terminals provide <10% of the synapses in layer 4, whereas the great majority of glutamatergic inputs come from layer 6 and 4 neurons (Peters and Payne, 1993; Ahmed et al., 1994, 1997). However, geniculate contribution is possibly higher in early development; thalamocortical development is characterized by pruning of inappropriate synapses (Katz and Shatz, 1996), whereas elaboration of appropriate arbors occurs without much synaptogenesis (Friedlander and Martin, 1989), and the density of cortical synapses in general gradually increases (Cragg, 1972; present study). Therefore, it is possible that the loss of NR2B occurs completely at thalamocortical terminals. The developmentally regulated replacement of NMDARs with AMPA receptors at a specific input may be the main factor that ends the ocular dominance plasticity. In addition, if future double labeling for thalamocortical terminals and glutamate receptor experiments would confirm this hypothesis, such findings may provide an anatomical basis for the loss of visually evoked NMDA-mediated responses by the end of the critical period in layer 4 (Tsumoto et al., 1987; Fox et al., 1989).

In conclusion, we propose that the presence of the NR2B subunit, possibly at the thalamocortical synapse, provides layer 4 of the visual cortex with the critical factor that renders this input plastic. We also propose that the loss of NR2B at the end of the critical period is a manifestation of the loss of functional NMDA receptor from this specific input and that this loss is instrumental in terminating the critical period of plasticity. Future experiments using ferrets reared in the dark are required to unveil a causative relationship between the end of the critical period and synaptic NR2B.

References

Ahmed B, Anderson JC, Douglas RJ, Martin KA, Nelson JC (1994) Polyneuronal innervation of spiny stellate neurons in cat visual cortex. J Comp Neurol 341:39–49.

Ahmed B, Anderson JC, Martin KA, Nelson JC (1997) Map of the synapses onto layer 4 basket cells of the primary visual cortex of the cat. J Comp Neurol 380:230–242.

Aoki C (1997) Postnatal changes in the laminar and subcellular distribution of NMDA-R1 subunits in the cat visual cortex as revealed by immunoelectron microscopy. Brain Res Dev Brain Res 98:41–59.

Bear MF, Kleinschmidt A, Gu QA, Singer W (1990) Disruption of experience-dependent synaptic modifications in striate cortex by infusion of an NMDA receptor antagonist. J Neurosci 10:909–925.

Buonomano DV, Merzenich MM (1998) Cortical plasticity: from synapses to maps. Annu Rev Neurosci 21:149–186.

Callaway EM, Lieber JL (1996) Development of axonal arbors of layer 6 pyramidal neurons in ferret primary visual cortex. J Comp Neurol 376:295–305.

Cao Z, Lickey ME, Liu L, Kirk E, Gordon B (2000a) Postnatal development of NR1, NR2A and NR2B immunoreactivity in the visual cortex of the rat. Brain Res 859:26–37.

Cao Z, Liu L, Lickey M, Gordon B (2000b) Development of NR1, NR2A and NR2B mRNA in NR1 immunoreactive cells of rat visual cortex. Brain Res 868:296–305.

Carmignoto G, Vicini S (1992) Activity-dependent decrease in NMDA receptor responses during development of the visual cortex. Science 258:1007–1011.

Chan J, Aoki C, Pickel VM (1990) Optimization of differential immunogold-silver and peroxidase labeling with maintenance of ultrastructure in brain sections before plastic embedding. J Neurosci Methods 33:113–127.

Chen L, Cooper NG, Mower GD (2000) Developmental changes in the expression of NMDA receptor subunits (NR1, NR2A, NR2B) in the cat visual cortex and the effects of dark rearing. Brain Res Mol Brain Res 78:196–200.

Colonnier M, Beaulieu C (1985) An empirical assessment of stereological formulae applied to the counting of synaptic disks in the cerebral cortex. J Comp Neurol 231:175–179.

Cragg BG (1972) The development of synapses in cat visual cortex. Invest Ophthalmol 11:377–385.

Currie SN, Wang XF, Daw NW (1994) NMDA receptors in layers II and III of rat cerebral cortex. Brain Res 662:103–108.

Daw NW (1994) Mechanisms of plasticity in the visual cortex: The Friedenwald Lecture. Invest Ophthalmol Vis Sci 35:4168–4179.

DeFelipe J, Marco P, Busturia I, Merchan-Perez A (1999) Estimation of the number of synapses in the cerebral cortex: methodological considerations. Cereb Cortex 9:722–732.

Durack JC, Katz LC (1996) Development of horizontal projections in layer 2/3 of ferret visual cortex. Cereb Cortex 6:178–183.

Erisir A, Van Horn SC, Bickford ME, Sherman SM (1997a) Immunocytochemistry and distribution of parabrachial terminals in the lateral geniculate nucleus of the cat: a comparison with corticogeniculate terminals. J Comp Neurol 377:535–549.

Erisir A, Van Horn SC, Sherman SM (1997b) Relative numbers of cortical and brainstem inputs to the lateral geniculate nucleus. Proc Natl Acad Sci USA 94:1517–1520.

Flint AC, Maisch US, Weishaupt JH, Kriegstein AR, Monyer H (1997) NR2A subunit expression shortens NMDA receptor synaptic currents in developing neocortex. J Neurosci 17:2469–2476.

Fox K, Sato H, Daw N (1989) The location and function of NMDA receptors in cat and kitten visual cortex. J Neurosci 9:2443–2454.

Fox K, Sato H, Daw N (1990) The effect of varying stimulus intensity on NMDA-receptor activity in cat visual cortex. J Neurophysiol 64: 1413–1428.

Friedlander MJ, Martin KA (1989) Development of Y-axon innervation of cortical area 18 in the cat. J Physiol (Lond) 416:183–213.

Gao WJ, Newman DE, Wormington AB, Pallas SL (1999) Development of inhibitory circuitry in visual and auditory cortex of postnatal ferrets: immunocytochemical localization of GABAergic neurons. J Comp Neurol 409:261–273.

Gilbert CD (1998) Adult cortical dynamics. Physiol Rev 78:467–485.

Godde B, Leonhardt R, Cords SM, Dinse HR (2002) Plasticity of orientation preference maps in the visual cortex of adult cats. Proc Natl Acad Sci USA 99:6352–6357.

Gu QA, Bear MF, Singer W (1989) Blockade of NMDA-receptors prevents ocularity changes in kitten visual cortex after reversed monocular deprivation. Brain Res Dev Brain Res 47:281–288.

Hubel DH, Wiesel TN, LeVay S (1977) Plasticity of ocular dominance columns in monkey striate cortex. Philos Trans R Soc Lond B Biol Sci 278:377–409.

Issa NP, Trachtenberg JT, Chapman B, Zahs KR, Stryker MP (1999) The critical period for ocular dominance plasticity in the ferret's visual cortex. J Neurosci 19:6965–6978.

Katz LC, Callaway EM (1992) Development of local circuits in mammalian visual cortex. Annu Rev Neurosci 15:31–56.

Katz LC, Shatz CJ (1996) Synaptic activity and the construction of cortical circuits. Science 274:1133–1138.

Kleinschmidt A, Bear MF, Singer W (1987) Blockade of "NMDA" receptors disrupts experience-dependent plasticity of kitten striate cortex. Science 238:355–358.

LeVay S, Wiesel TN, Hubel DH (1980) The development of ocular dominance columns in normal and visually deprived monkeys. J Comp Neurol 191:1–51.

Locke M (1994) Preservation and contrast without osmication or section staining. Microsc Res Tech 29:1–10.

Lu HC, Gonzalez E, Crair MC (2001) Barrel cortex critical period plasticity is independent of changes in NMDA receptor subunit composition. Neuron 32:619–634.

Monyer H, Sprengel R, Schoepfer R, Herb A, Higuchi M, Lomeli H, Burnashev N, Sakmann B, Seeburg PH (1992) Heteromeric NMDA receptors: molecular and functional distinction of subtypes. Science 256:1217–1221.

Monyer H, Burnashev N, Laurie DJ, Sakmann B, Seeburg PH (1994) Developmental and regional expression in the rat brain and functional properties of four NMDA receptors. Neuron 12:529–540.

Peters A, Payne BR (1993) Numerical relationships between geniculocortical afferents and pyramidal cell modules in cat primary visual cortex. Cereb Cortex 3:69–78.

Phend KD, Weinberg RJ, Rustioni A (1992) Techniques to optimize post-embedding single and double staining for amino acid neurotransmitters. J Histochem Cytochem 40:1011–1020.

Phend KD, Rustioni A, Weinberg RJ (1995) An osmium-free method of EPON embedment that preserves both ultrastructure and antigenicity for post-embedding immunocytochemistry. J Histochem Cytochem 43:283–292.

Philpot BD, Weisberg MP, Ramos MS, Sawtell NB, Tang YP, Tsien JZ, Bear MF (2001) Effect of transgenic overexpression of NR2B on NMDA receptor function and synaptic plasticity in visual cortex. Neuropharmacology 41:762–770.

Portera-Cailliau C, Price DL, Martin LJ (1996) *N*-methyl-D-aspartate receptor proteins NR2A and NR2B are differentially distributed in the developing rat central nervous system as revealed by subunit-specific antibodies. J Neurochem 66:692–700.

Quinlan EM, Olstein DH, Bear MF (1999) Bidirectional, experience-dependent regulation of *N*-methyl-D-aspartate receptor subunit composition in the rat visual cortex during postnatal development. Proc Natl Acad Sci USA 96:12876–12880.

Rauschecker JP (1991) Mechanisms of visual plasticity: Hebb synapses, NMDA receptors, and beyond. Physiol Rev 71:587–615.

Roberts EB, Ramoa AS (1999) Enhanced NR2A subunit expression and decreased NMDA receptor decay time at the onset of ocular dominance plasticity in the ferret. J Neurophysiol 81:2587–2591.

Roberts EB, Meredith MA, Ramoa AS (1998) Suppression of NMDA receptor function using antisense DNA block ocular dominance plasticity while preserving visual responses. J Neurophysiol 80:1021–1032.

Sheng M, Cummings J, Roldan LA, Jan YN, Jan LY (1994) Changing subunit composition of heteromeric NMDA receptors during development of rat cortex. Nature 368:144–147.

Shirokawa T, Nishigori A, Kimura F, Tsumoto T (1989) Actions of excitatory amino acid antagonists on synaptic potentials of layer II/III neurons of the cat's visual cortex. Exp Brain Res 78:489–500.

Stern EA, Maravall M, Svoboda K (2001) Rapid development and plasticity of layer 2/3 maps in rat barrel cortex in vivo. Neuron 31:305–315.

Tsumoto T, Hagihara K, Sato H, Hata Y (1987) NMDA receptors in the visual cortex of young kittens are more effective than those of adult cats. Nature 327:513–514.

Van Horn SC, Erisir A, Sherman SM (2000) Relative distribution of synapses in the A-laminae of the lateral geniculate nucleus of the cat. J Comp Neurol 416:509–520.

Weinberger NM (1995) Dynamic regulation of receptive fields and maps in the adult sensory cortex. Annu Rev Neurosci 18:129–158.

Williams K, Russell SL, Shen YM, Molinoff PB (1993) Developmental switch in the expression of NMDA receptors occurs in vivo and in vitro. Neuron 10:267–278.